

AEM: Attention Entropy Maximization for Multiple Instance Learning based Whole Slide Image Classification

Yunlong Zhang^{1,2}, Zhongyi Shui^{1,2}, Yunxuan Sun^{1,2}, Honglin Li^{1,2}, Jingxiong Li^{1,2}, Chenglu Zhu²,
Lin Yang^{2*}

¹College of Computer Science and Technology, Zhejiang University, China

²Research Center for Industries of the Future and School of Engineering, Westlake University, China
{zhangyunlong,yanglin}@westlake.edu.cn

Abstract

Multiple Instance Learning (MIL) has demonstrated effectiveness in analyzing whole slide images (WSIs), yet it often encounters overfitting challenges in real-world applications, particularly in the form of attention over-concentration. While existing methods to alleviate this issue introduce complex modules or processing steps, such as multiple-stage training and teacher-student distillation, this paper proposes a simple yet effective regularization: Attention Entropy Maximization (AEM). Motivated by our investigation revealing a positive correlation between attention entropy and model performance, AEM incorporates a negative entropy loss for attention values into the standard MIL framework, penalizing overly concentrated attention and encouraging the model to consider a broader range of informative regions in WSIs, potentially improving its generalization capabilities. Compared to existing overfitting mitigation methods, our AEM approach offers advantages of simplicity, efficiency, and versatility. It requires no additional modules or processing steps, involves only one hyperparameter, and demonstrates compatibility with MIL frameworks and techniques. These advantages make AEM particularly attractive for practical applications. We evaluate AEM on three benchmark datasets, demonstrating consistent performance improvements over existing methods. Furthermore, AEM shows high versatility, integrating effectively with four feature extractors, two advanced MIL frameworks, three attention mechanisms, and Subsampling augmentation technique. The source code is available at <https://github.com/dazhangyu123/AEM>.

Introduction

Whole slide images (WSIs) are widely recognized as the gold standard for numerous cancer diagnoses, playing a crucial role in ensuring precise diagnosis (Bejnordi et al. 2017), prognosis (Li et al. 2018; Yao et al. 2020), and the development of treatment plans (Song et al. 2023). In recent years, attention-based multiple instance learning (AB-MIL) has emerged as a promising approach for WSI analysis (Ding et al. 2023; Myronenko et al. 2021; Li et al. 2021; Zheng et al.; Yang et al. 2022; Zhang et al. 2022b; Guo et al.; Li et al. 2023b,a). However, recent studies have uncovered overfitting issues in MIL due to factors like limited available data (Tang et al. 2023; Zhang et al. 2022a, 2024; Li, Li,

and Eliceiri 2021), class imbalance (Zhang et al. 2024), and staining bias (Lin et al. 2023; Zhang et al. 2022c).

In the attention mechanism, attention values represent the importance or relevance of different instances to the bag prediction, influencing both prediction accuracy and result interpretability. Multiple relevant studies (Lu et al. 2021; Shao et al. 2021; Tang et al. 2023; Yufei et al. 2022; Zhang et al. 2024) have revealed that excessive concentration of attention values in ABMIL methods hinders model interpretability and results in overfitting (Zhang et al. 2024). There have been several solutions for alleviating attention concentration. Masking-based methods (Qu et al. 2022; Tang et al. 2023; Zhang et al. 2024) mask out the instances with the highest attention values, allocating their attention values to remaining instances. Clustering-based methods (Sharma et al. 2021; Guan et al. 2022) group instances into clusters and randomly sample instances from these clusters, ensuring attention values are not overly focused on minority instances. MBA (Zhang et al. 2024) generates the heatmap by averaging the attention values generated by multiple attention heads, thereby avoiding the over-concentration of attention values. While these methods show promise, they often introduce complex modules or processing steps, increasing computational time and limiting flexibility (refer to Table 1).

To overcome the limitations of existing complex solutions, this paper introduces Attention Entropy Maximization (AEM), a simple yet effective technique to mitigate attention concentration and MIL method overfitting. Our investigation reveals a positive correlation between attention entropy and model performance, motivating the development of AEM. This approach incorporates a negative entropy loss for attention values into the standard MIL framework (Figure 1), promoting a more uniform distribution of attention across instances. This encourages the model to consider a broader range of informative regions in WSIs, potentially improving its generalization capabilities. Compared to existing methods, AEM offers several advantages: 1) it requires no additional modules or processing steps, 2) it involves only one hyperparameter, and 3) it exhibits good versatility.

Our experimental evaluations on three benchmark datasets (CAMELYON16, CAMELYON17, and our in-house LBC dataset) demonstrate AEM’s superior performance over existing methods. Furthermore, extensive experiments showcase AEM’s versatility, effectively combin-

*Corresponding author

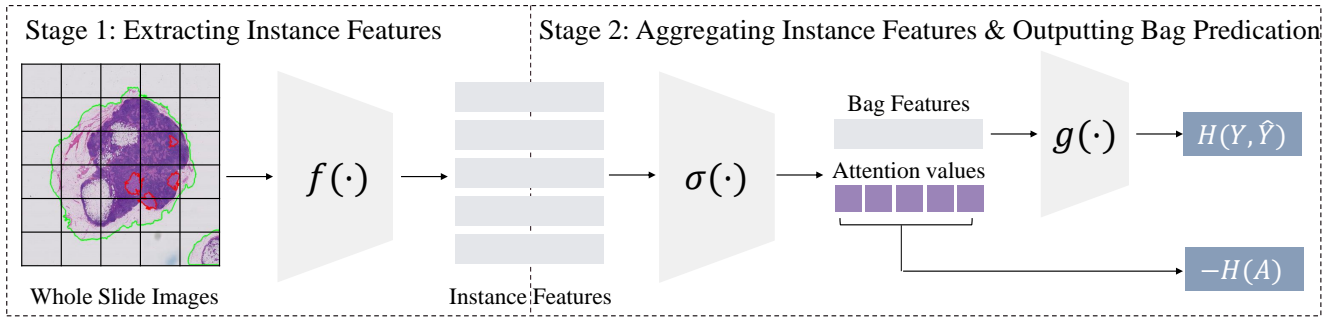


Figure 1: Overview of plugging AEM into MIL framework. AEM adds only a negative entropy regularization for attention values to the regular MIL framework.

ing with four feature extractors, Subsampling augmentation technique, two advanced MIL frameworks, and three attention mechanisms. These results underscore AEM’s potential as a widely applicable enhancement to existing MIL methodologies in medical image analysis.

Related Work

MIL for WSI classification

Multiple Instance Learning (MIL) is a powerful approach for whole slide image (WSI) classification, where a single WSI is divided into smaller patches with an overall label for the slide but unknown labels for individual patches. Traditional MIL methods, such as mean-pooling and max-pooling, aggregate information from patches by averaging all patch features or selecting the most significant feature, respectively, but these methods fail to account for the varying importance of different patches. Attention-based MIL (ABMIL) (Ilse, Tomczak, and Welling 2018) addresses this limitation by using an attention mechanism to assign different weights to patches based on their relevance to the classification task, thus focusing on the most informative regions. Over the years, several improvements have been made to enhance ABMIL: hierarchical attention mechanisms (Zhang et al. 2022a, 2024) capture both local and global contexts, self-supervised learning (Dehaene et al. 2020; Lu et al. 2021; Wang et al. 2022) techniques improve feature representations through pretext tasks, graph-based methods (Chan et al.; Guan et al. 2022; Zhao et al. 2020, 2023) model spatial relationships between patches more effectively, transformer models (Shao et al. 2021; Xiong et al. 2023; Li et al. 2023a, 2024; Ma et al. 2024) leverage powerful attention mechanisms to handle long-range dependencies, data augmentation methods (Lin et al. 2024; Keum et al. 2023; Gadermayr et al. 2023; Zhang et al. 2022a; Yang et al. 2022) to increase the size of training samples, and multi-scale approaches (Li, Li, and Eliceiri 2021; Hou et al. 2022; Bontempo et al. 2023) analyze patches at different magnifications to integrate fine-grained details with broader contextual information.

Attention concentration for MIL

Despite the success of ABMIL and its variants, several studies (Li, Li, and Eliceiri 2021; Zhang et al. 2024) have revealed that attention values in ABMIL tend to concentrate on a small number of instances, diverging from pathologists’

tumor region annotations. Moreover, a recent study (Zhang et al. 2024) has shown that excessive concentration of attention values will lead to model overfitting.

Various methods have been proposed to alleviate attention concentration. WENO (Qu et al. 2022) and MHIM-MIL (Tang et al. 2023) propose hard positive instance mining strategies. ACMIL (Zhang et al. 2024) introduces multiple attention branches and instance masking. While these methods show promise, they often introduce complex modules or processing steps, increasing computational complexity and potentially limiting their applicability. In contrast, our proposed AEM method directly applies regularization to disperse attention values, offering a simpler, more efficient, and versatile solution to the attention concentration problem. A preliminary comparison is shown in Table 1.

Entropy regularization

Entropy, a concept originating from information theory, quantifies the uncertainty or disorder within a system (Shannon 1948). In the context of probability distributions, entropy measures the unpredictability of a random variable. Mathematically, for a discrete random variable X with probability mass function $P(X)$, the entropy $H(X)$ is defined as:

$$H(X) = - \sum_x P(x) \log P(x).$$

This measure has been pivotal in various fields, including thermodynamics, information theory, and more recently, machine learning and deep learning.

In deep learning, entropy regularization has been widely used to encourage models to produce more uncertain or smoother predictions, leading to improved generalization and robustness. It has been successfully applied in various fields, including Semi-Supervised Learning (Grandvalet and Bengio 2004), Adversarial Training (Miyato et al. 2018), Reinforcement Learning (Schulman et al. 2017), Generative Models (Kingma and Welling 2013), and Domain Adaptation (Saito et al. 2019).

However, unlike common applications of entropy regularization to model predictions, our AEM method uniquely applies entropy regularization to attention values in MIL. This novel approach addresses the specific challenge of attention

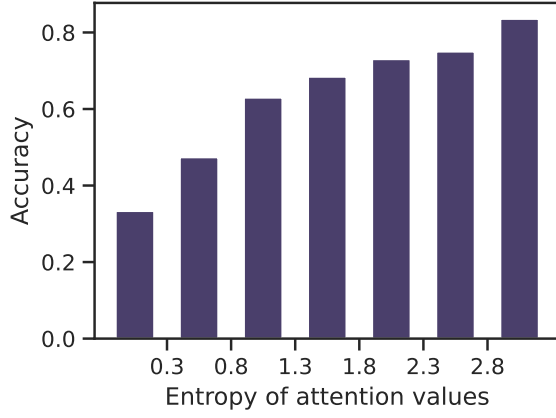


Figure 2: Samples with higher entropy in their attention values exhibit higher accuracy. This result is obtained on the LBC dataset at seed 1.

concentration in WSI classification, promoting a more diverse distribution of attention across instances and potentially improving model generalization.

Method

We present AEM, a plug-and-play regularization technique to enhance the MIL framework. We introduce AEM based on the widely used ABMIL framework (see Figure 1). In the Supplementary Material, we also provide instructions for integrating AEM with Subsampling, DTFD-MIL, ACMIL, MHA, and DSMIL. This section is structured as follows: an overview of ABMIL for WSI classification, the motivation behind AEM, the implementation of AEM, and three noteworthy properties of AEM.

ABMIL for WSI Analysis

MIL formulation. For the WSI classification problem, we have access to the WSI X along with its slide-level label Y . Typically, the resolution of a WSI ranges from $50,000 \times 50,000$ to $100,000 \times 100,000$, making it computationally infeasible to be directly used for training. To resolve this, regular MIL framework, represented by ABMIL (Ilse, Tomczak, and Welling 2018), segments full resolution WSIs into non-overlapping patches $\{x_n\}_{n=1}^N$, following applying a two-step process to predict the slide label \hat{Y} . Next, we provide a detailed introduction to these two steps.

Extracting instance feature. Due to computational limitations, current MIL methods often use features extracted from a frozen backbone like an ImageNet-pretrained ResNet. Recent research (Lu et al. 2021; Dehaene et al. 2020) has shown that replacing this encoder with one pre-trained using Self-Supervised Learning (SSL) can lead to significant performance improvements. Moreover, recent studies indicate that Visual-Language Pretraining (VLP) (Huang et al. 2023; Lu et al. 2024; Ikezogwo et al. 2024; Sun et al. 2024b,a) can learn more powerful and rich representations by aligning pathology images with text. To verify the versatility of our AEM, we employ four types of

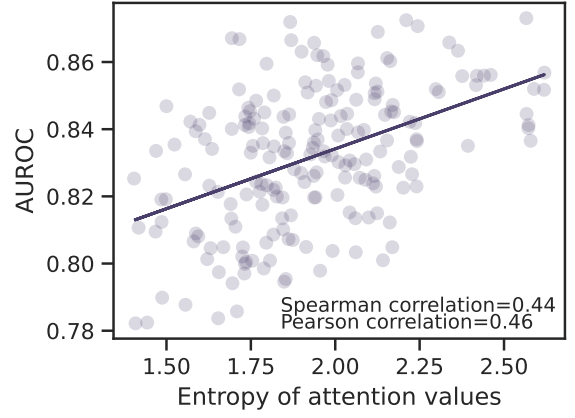


Figure 3: There exists a moderate positive correlation between AUROC values and entropy of attention values across experimental seeds. One point denotes the outcome of a single seed on the LBC dataset.

feature extractors, including ResNet18 pre-trained by supervised learning, ViT-S/16 pre-trained by DINO (Kang et al. 2023), ViT-B/16 pre-trained by PathGen-CLIP (Sun et al. 2024a), and ViT-L/14 pre-trained by PathGen-CLIP (Sun et al. 2024a).

Aggregating instance features and outputting bag prediction. ABMIL aggregates all instance embeddings into the bag embedding using a gated attention operator, which can be written as:

$$z = \sum_{n=1}^N a_n h_n, \quad (1)$$

where $a_n = \sigma(h_n)$ represents the attention values for n -th instance, h_n . Specifically, the gated attention mechanism $\sigma(h_n)$ can be formulated as:

$$\sigma(h_n) = \frac{\exp\{w^T(\tanh(V_1 h_n) \odot \text{sigm}(V_2 h_n))\}}{\sum_{j=1}^N \exp\{w^T(\tanh(V_1 h_j) \odot \text{sigm}(V_2 h_j))\}}, \quad (2)$$

where $V_1, V_2 \in \mathbb{R}^{L \times M}$, $w \in \mathbb{R}^{L \times 1}$ are parameters, \odot is an element-wise multiplication and $\text{sigm}(\cdot)$ is the sigmoid non-linearity. Obtaining the bag embedding, ABMIL outputs the bag prediction by suspending a MLP layer $\hat{Y} = g(z)$. The loss for training the ABMIL is defined as:

$$L_{ce} = H(Y, \hat{Y}) = - \sum_i Y_i \log \hat{Y}_i. \quad (3)$$

Motivation of AEM

Extensive studies have demonstrated that low attention entropy can lead to instability in the training process and poor model generalization for attention based models (Zhai et al. 2023; Radford et al. 2019; Xiong et al. 2020; Dehghani et al. 2023). To illustrate this issue more clearly in the WSI classification task, we plotted the relationship between attention entropy and ABMIL’s performance. In Figure 2, we observed that samples with higher entropy in their attention

Table 1: Detailed comparison of methods used for combating the overfitting for WSI classification. **Time** means the training time cost on CAMELYON-16 dataset. **Num. of hyper** denotes the number of hyperparameters introduced by methods.

Method	Extra Modules/Processing	Time	Num. of hyper
DTFD-MIL (Zhang et al. 2022a)	Double-tier attention mechanisms	12.7 min	2
IBMIL (Lin et al. 2023)	New training stage of interventional training from scratch	19.9 min	1
C2C (Sharma et al. 2021)	Clustering and sampling process	-	4
MHIM-MIL (Tang et al. 2023)	Teacher model for masking easy instances	21.8 min	6
ACMIL (Zhang et al. 2024)	Multiple branch attention for extracting pattern embeddings	12.5 min	3
AEM(ours)	None	10.5 min	1

values tended to demonstrate higher accuracy. Figure 3 illustrates the positive correlation between AUROC and the entropy of attention values across experimental seeds. These findings underscore the importance of maintaining high attention entropy for improved model performance and generalization in WSI classification tasks.

Attention Entropy Maximization

The objective of AEM is to maximize the entropy $H(A)$ of attention values, $A = \{a_n\}_{n=1}^N$. This is achieved by formulating AEM as the negative entropy (Shannon 1948):

$$L_{aem} = -H(A) = -\sum_n a_n \log a_n. \quad (4)$$

This formulation encourages the model to consider a broader range of informative regions in WSIs, potentially improving its generalization capabilities. By combining Eq. 3 and 4, the final objective of our solution can be formulated as:

$$L_{total} = L_{ce} + \lambda L_{aem}, \quad (5)$$

where λ is a hyperparameter that balances the trade-off between L_{ce} and L_{aem} . We emphasize that λ plays a key role in the application of AEM. On one hand, a too small λ means the regularization is negligible. On the other hand, setting λ too large causes the attention model to degrade to mean-pooling, which has been demonstrated to be sub-optimal. We explore the role of λ across three datasets in the ablation study. In practice, we determine the optimal λ based on the validation performance.

Discussion. AEM serves a similar role to the KL-divergence loss in the C2C (Sharma et al. 2021) by assigning attention values to more patches. However, there are distinct differences between them. Firstly, while AEM operates on all instances, the KL-divergence loss in C2C focuses on instances within a cluster. Secondly, the negative entropy is independent of any reference distribution and directly penalizes peaked distributions, whereas the KL-divergence loss explicitly uses a uniform distribution as a reference and encourages the attention to be closer to uniform. This disparity makes the KL-divergence loss unsuitable as our objective (validated in the ablation study).

Properties of AEM

Requiring no additional modules or processing steps. Unlike many existing methods in MIL for WSI classification that introduce extra auxiliary modules or processing

stages, AEM achieves superior performance without additional components or computational overhead. This simplicity makes AEM both efficient and straightforward to implement. As shown in Table 1, AEM’s computational cost is significantly lower than other advanced MIL methods.

Requiring only one hyperparameter. AEM introduces only one hyperparameter, λ , which balances the classification loss and regularization loss. In contrast, most advanced methods (except IBMIL) require tuning multiple parameters (see Table 1). This single-parameter design simplifies the model’s optimization process and reduces computational complexity, making AEM more accessible and easier to adapt to different datasets or applications.

Good Versatility. AEM’s simplicity enables its integration with various MIL methods. In principle, AEM can effectively improve performance wherever attention concentration exists in the baseline. We demonstrate AEM’s versatility in four ways: 1) by combining it with the data augmentation technique, Subsampling, 2) by integrating it with two advanced MIL frameworks, DTFD-MIL (Zhang et al. 2022a) and ACMIL (Zhang et al. 2024), 3) by integrating it with extra attention mechanisms, DSMIL (Li, Li, and Elieiri 2021) and MHA (Vaswani et al. 2017), and 4) by integrating it with various feature extractors, ImageNet pretrained ResNet, SSL pretrained ViT, and VLP pretrained ViT.

Experiments

Experimental setup

The experimental setup is placed in Supplementary Material, including the introduction of datasets and experimental details.

Main results

Performance comparison with SOTA methods. Table 2 presents a comprehensive comparison of various MIL approaches across three datasets (CAMELYON-16, CAMELYON-17, and LBC) using two different pretraining methods (SSL pretrained ViT-S and VLP pretrained ViT-L) and two evaluation metrics (F1-score and AUC).

A key finding is that AEM, the proposed method, achieves superior performance on F1-scores, surpassing other methods across all scenarios. This consistent excellence in F1-score highlights AEM’s balanced performance in precision and recall.

Table 2: The performance of different MIL approaches across three datasets and two evaluation metrics. The most superior performance is highlighted in **bold**.

SSL pretrained ViT-S (Lunit (Kang et al. 2023))						
Method	CAMELYON-16		CAMELYON-17		LBC	
	F1-score	AUC	F1-score	AUC	F1-score	AUC
Max-pooling	0.903 \pm 0.054	0.956 \pm 0.029	0.413 \pm 0.077	0.722 \pm 0.069	0.590 \pm 0.043	0.829 \pm 0.023
Mean-pooling	0.577 \pm 0.057	0.569 \pm 0.081	0.402 \pm 0.026	0.751 \pm 0.015	0.559 \pm 0.024	0.827 \pm 0.012
Clam-SB (Lu et al. 2021)	0.925 \pm 0.035	0.969 \pm 0.024	0.523 \pm 0.020	0.846 \pm 0.020	0.617 \pm 0.022	0.865 \pm 0.018
LossAttn (Shi et al. 2020)	0.908 \pm 0.031	0.928 \pm 0.014	0.575 \pm 0.051	0.865 \pm 0.016	0.621 \pm 0.012	0.843 \pm 0.006
TransMIL (Shao et al. 2021)	0.922 \pm 0.019	0.943 \pm 0.009	0.554 \pm 0.048	0.792 \pm 0.029	0.539 \pm 0.028	0.805 \pm 0.010
DSMIL (Li, Li, and Eliceiri 2021)	0.943 \pm 0.007	0.966 \pm 0.009	0.532 \pm 0.064	0.804 \pm 0.032	0.562 \pm 0.028	0.820 \pm 0.033
IBMIL (Lin et al. 2023)	0.912 \pm 0.034	0.954 \pm 0.022	0.557 \pm 0.034	0.850 \pm 0.024	0.604 \pm 0.032	0.834 \pm 0.014
MHIM-MIL (Tang et al. 2023)	0.932 \pm 0.024	0.970\pm0.037	0.541 \pm 0.022	0.845 \pm 0.026	0.658 \pm 0.041	0.872 \pm 0.022
ILRA (Xiang and Zhang 2022)	0.904 \pm 0.071	0.940 \pm 0.060	0.631 \pm 0.051	0.860 \pm 0.020	0.618 \pm 0.051	0.859 \pm 0.017
ABMIL (Ilse, Tomczak, and Welling 2018)	0.914 \pm 0.031	0.945 \pm 0.027	0.522 \pm 0.050	0.853 \pm 0.016	0.595 \pm 0.036	0.831 \pm 0.022
AEM(ours)	0.951\pm0.004	0.967 \pm 0.008	0.638\pm0.007	0.883\pm0.013	0.664\pm0.021	0.874\pm0.012
VLP pretrained ViT-L (PathGen-CLIP (Sun et al. 2024a))						
Method	CAMELYON-16		CAMELYON-17		LBC	
	F1-score	AUC	F1-score	AUC	F1-score	AUC
max-pooling	0.948 \pm 0.014	0.975 \pm 0.011	0.513 \pm 0.081	0.790 \pm 0.042	0.617 \pm 0.029	0.855 \pm 0.020
min-pooling	0.585 \pm 0.079	0.653 \pm 0.098	0.460 \pm 0.026	0.787 \pm 0.010	0.596 \pm 0.009	0.843 \pm 0.011
Clam-SB (Lu et al. 2021)	0.941 \pm 0.014	0.960 \pm 0.015	0.622 \pm 0.031	0.899 \pm 0.012	0.641 \pm 0.025	0.870 \pm 0.013
LossAttn (Shi et al. 2020)	0.948 \pm 0.004	0.981 \pm 0.017	0.667 \pm 0.023	0.891 \pm 0.009	0.657 \pm 0.035	0.874 \pm 0.006
TransMIL (Shao et al. 2021)	0.951 \pm 0.024	0.968 \pm 0.028	0.656 \pm 0.021	0.892 \pm 0.014	0.573 \pm 0.019	0.849 \pm 0.010
DSMIL (Li, Li, and Eliceiri 2021)	0.895 \pm 0.038	0.949 \pm 0.017	0.582 \pm 0.062	0.887 \pm 0.013	0.586 \pm 0.024	0.848 \pm 0.010
IBMIL (Lin et al. 2023)	0.935 \pm 0.014	0.953 \pm 0.009	0.629 \pm 0.027	0.884 \pm 0.016	0.640 \pm 0.010	0.867 \pm 0.007
MHIM-MIL (Tang et al. 2023)	0.946 \pm 0.033	0.984 \pm 0.016	0.594 \pm 0.090	0.912 \pm 0.009	0.660 \pm 0.030	0.890\pm0.007
ILRA (Xiang and Zhang 2022)	0.929 \pm 0.018	0.963 \pm 0.019	0.662 \pm 0.048	0.914\pm0.017	0.626 \pm 0.028	0.864 \pm 0.014
ABMIL (Ilse, Tomczak, and Welling 2018)	0.953 \pm 0.018	0.972 \pm 0.010	0.610 \pm 0.025	0.864 \pm 0.017	0.621 \pm 0.023	0.853 \pm 0.013
AEM(ours)	0.967\pm0.025	0.987\pm0.013	0.676\pm0.016	0.903 \pm 0.005	0.683\pm0.032	0.882 \pm 0.010

With SSL pretrained ViT-S, AEM achieves the highest F1-scores for all three datasets and the highest AUC for CAMELYON-17 and LBC. On CAMELYON-16, MHIM-MIL slightly outperforms AEM in AUC.

Using VLP pretrained ViT-L, AEM maintains its superiority in F1-scores across all datasets. However, its AUC performance shows some variability. For CAMELYON-16, AEM leads in both F1-score and AUC. On CAMELYON-17, AEM has the highest F1-score, but ILRA slightly outperforms it in AUC. For LBC, AEM again leads in F1-score, but MHIM-MIL achieves a marginally higher AUC.

Versatility of AEM

AEM’s effectiveness across different feature extractors.

Table 2 demonstrates that our AEM consistently enhances the performance of ABMIL using both SSL pretrained ViT-S (Kang et al. 2023) and VLP pretrained ViT-L (Sun et al. 2024a). Furthermore, in the Supplementary Material, we report similar performance gains using ImageNet pretrained ResNet18 and VLP pretrained ViT-B, further demonstrating AEM’s versatility across various architectures and pretraining strategies.

AEM amplifies and complements Subsampling augmentation. Figure 4a illustrates the impact of Subsampling

(Keum et al. 2023; Keshvarikhajasteh, Pluim, and Veta 2024) and AEM on model performance across various datasets and pretrained configurations.

Subsampling generally improves upon the ABMIL baseline. However, its effectiveness varies, suggesting dataset-specific biases. Notable improvements are observed in CAMELYON17/VLP (AUROC increase from 0.86 to 0.90) and LBC/VLP (0.79 to 0.82). However, subsampling shows marginal gains in CAMELYON16 datasets and even a slight performance drop in CAMELYON17/SSL (0.85 to 0.84).

AEM consistently enhances performance beyond subsampling alone, particularly in scenarios where subsampling had a minimal impact (e.g., CAMELYON17/SSL: AUROC increase from 0.85 to 0.89). Moreover, even in cases where subsampling was already effective, AEM still elevates performance. This consistent pattern suggests that AEM effectively addresses some limitations of subsampling, providing a robust method to enhance model performance across diverse settings.

AEM amplifies and complements upon advanced MIL frameworks, DTFD-MIL and ACMIL. DTFD-MIL (Zhang et al. 2022a) and ACMIL (Zhang et al. 2024) are two advanced MIL frameworks that improve upon ABMIL. As shown in Figure 4b and 4c, DTFD-MIL and ACMIL signif-

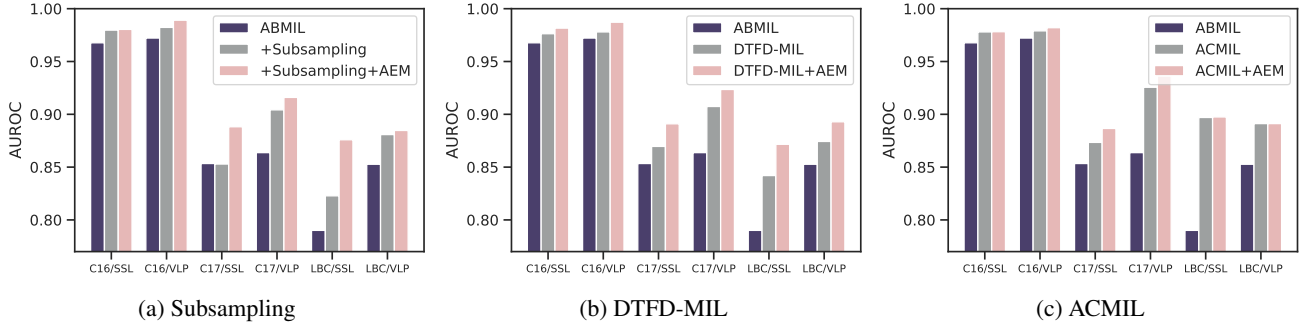


Figure 4: Performance comparison before and after plugging AEM into the Subsampling augmentation (a) and two advanced MIL frameworks, DTFD-MIL (b) and AC MIL (c). C17/SSL indicates results on CAMELYON17 using an SSL-pretrained backbone. AEM improves their performance on 17 out of 18 terms.

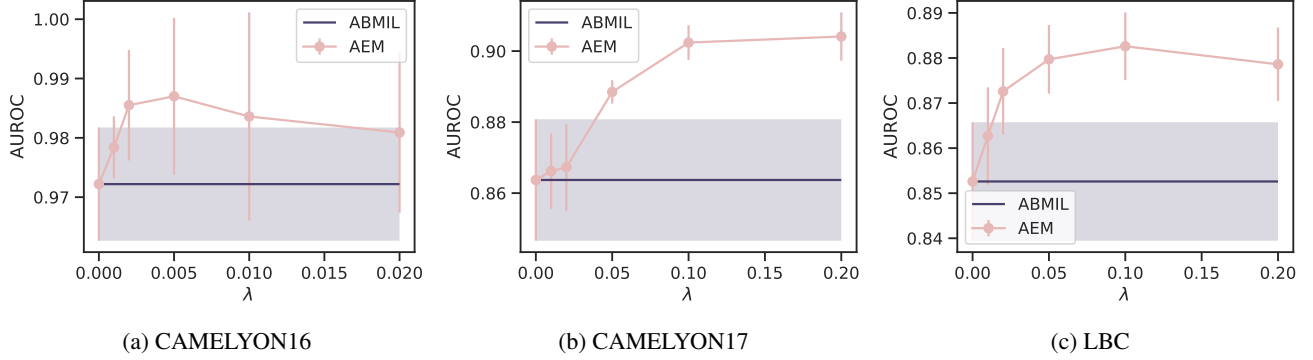


Figure 5: Sensitivity analysis of hyperparameter λ across the three datasets. Both smaller and larger values of λ yield sub-optimal performance, highlighting the critical importance of selecting an appropriate λ for AEM.

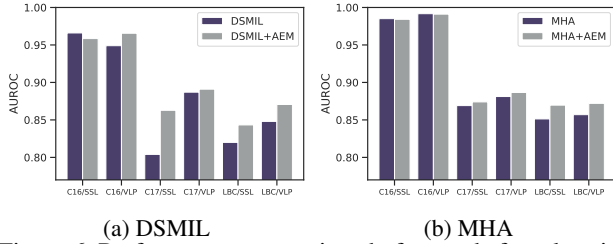


Figure 6: Performance comparison before and after plugging AEM into two attention mechanisms, DSMIL and MHA. AEM can improve their performance on 9 out of 12 terms.

icantly enhance AUC compared to ABMIL, and integrating our AEM further improves their performance. To better understand the impact of AEM on these advanced frameworks, we analyze its effects on each method separately.

For DTFD-MIL, The integration of AEM consistently improves AUC across three datasets (CAMELYON16, CAMELYON17, and LBC) and two pre-trained backbones (SSL and VLP). The enhancement is particularly pronounced on the CAMELYON17 and LBC datasets, where we observe an AUC increase of approximately 2%, highlighting AEM's effectiveness in challenging scenarios.

For AC MIL, while AC MIL was designed to alleviate attention concentration, playing a similar role to AEM, the integration of AEM still enhances its performance. On CAMELYON16 and CAMELYON17 datasets, AC MIL+AEM shows consistent improvements over AC MIL alone. For the LBC dataset, AC MIL+AEM

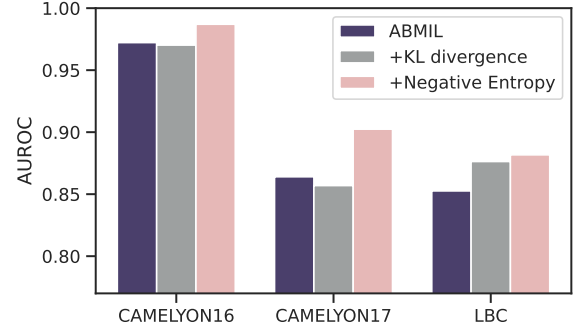
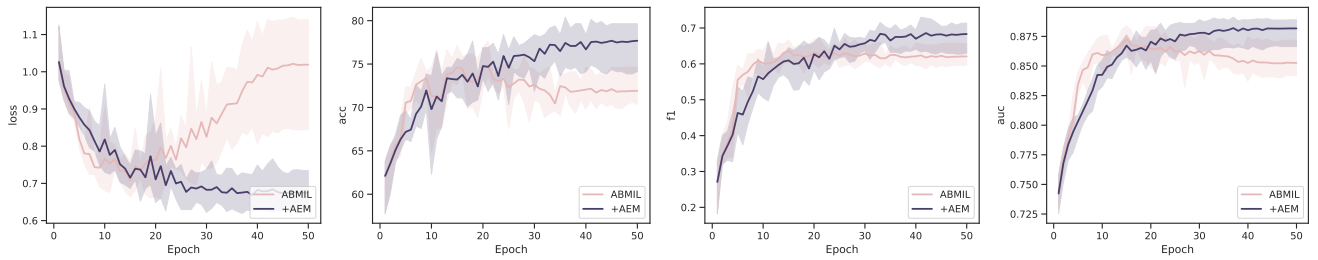


Figure 7: Performance comparison of using negative entropy and KL divergence as the loss formulation of AEM. Negative entropy is more suitable for AEM.

achieves comparable performance to AC MIL.

Performance gains of AEM across different attention mechanisms. Our main results demonstrate the effectiveness of AEM on gated attention. To further validate its versatility, we applied AEM to two additional attention mechanisms beyond gated attention in ABMIL: DSMIL (Li, Li, and Eliceiri 2021) and MHA (Zhang et al. 2024). Figure 6 illustrates AEM's impact on these mechanisms across various datasets and feature extraction methods.

For DSMIL, AEM's effectiveness varies by dataset and feature type. Significant improvements are observed for CAMELYON17/SSL and LBC datasets, while CAMELYON16/SSL performs slightly better without AEM. No-



(a) Test Loss

(b) Test Accuracy

(c) Test F1-score

(d) Test AUROC

Figure 8: Performance comparison between ABMIL (Ilse, Tomczak, and Welling 2018) and our AEM on LBC test set throughout the training process. ABMIL displays pronounced signs of overfitting, as indicated by a significant increase in validation loss and a decline in the other three evaluation metrics. Conversely, AEM effectively mitigates the overfitting issue.

tably, AEM consistently enhances DSMIL’s performance with VLP features across all datasets.

For MHA, AEM’s impact is generally positive but more subtle. Slight improvements are seen in CAMELYON17 and LBC datasets, with minimal changes in CAMELYON16 datasets. The less pronounced effect on MHA and DSMIL compared to gated attention may be attributed to these mechanisms’ inherent ability to learn diverse attention values (Li, Li, and Eliceiri 2021; Zhang et al. 2024).

Overall, while AEM’s effectiveness varies, it shows particular promise for DSMIL with VLP features and for more challenging datasets like CAMELYON17 and LBC. These findings suggest that AEM’s utility may depend on the specific attention mechanism, feature representation, and dataset complexity, highlighting the need for careful consideration in its application to different WSI analysis scenarios.

Ablation Study

Sensitivity analysis to hyperparameter λ . We conducted the ablation study on three datasets to examine the role of the hyperparameter of λ . Due to the space limitation, we placed the SSL pre-trained results at supplementary material. We varied λ across a range of values: $\{0, 0.01, 0.02, 0.05, 0.1, 0.2\}$ on CAMELYON17 and LBC datasets, and varied λ across a range of values: $\{0, 0.001, 0.002, 0.005, 0.01, 0.02\}$ on CAMELYON16 dataset. Here, $\lambda = 0$ indicates the exclusion of AEM. As depicted in Figure 5, setting $\lambda > 0$ consistently enhances performance compared to the baseline ($\lambda = 0$) on all three datasets. Moreover, different λ should be set for different datasets to achieve the best performance. Specifically, $\lambda = 0.005$ for CAMELYON16, $\lambda = 0.2$ for CAMELYON17, and $\lambda = 0.1$ for LBC. Thus, selecting an appropriate λ is crucial for optimizing the effectiveness of AEM.

Superiority of Negative Entropy over KL Divergence in AEM Loss Formulation. To compare their difference as the loss formulation for AEM, we compare AUROC results across three datasets on VLP pretrained embeddings. Figure 7 presents the performance of ABMIL, ABMIL with negative entropy, and ABMIL with KL divergence. The negative entropy formulation consistently outperformed both baseline and KL divergence variants across all datasets. KL divergence showed mixed results, improving baseline performance on LBC but degrading on CAMELYON datasets.

Overall, negative entropy demonstrates more consistent and stable performance improvements, suggesting it is the preferred loss formulation for AEM.

Further analysis

AEM effectively mitigates the overfitting. Figure 8 compares ABMIL (red) and AEM (purple) performance across four metrics during training: Figure 8a (test Loss): AEM shows a more stable, lower loss, while ABMIL’s loss increases after 20 epochs, suggesting overfitting. Figure 8b (test Accuracy): AEM maintains higher accuracy throughout, while ABMIL plateaus and slightly decreases after 30 epochs. Figure 8c (test F1-score) and Figure 8d (test AUROC): AEM consistently outperforms ABMIL, reaching higher peaks and maintaining stability. ABMIL shows slight performance degradation in later epochs. Overall, AEM shows better generalization and more robust performance across all metrics, indicating its potential as a more reliable method that’s less prone to overfitting compared to ABMIL.

Additional results. Further results are presented in the Supplementary Material, including: (1) evaluation metric curves demonstrating how ADR mitigates attention over-concentration, (2) heatmap visualizations showcasing improved interpretability, (3) UMAP visualizations of bag features illustrating AEM’s ability to learn more discriminative representations, and (4) a comprehensive analysis of AEM’s integration with DTFD-MIL, ACMIL, and Subsampling, considering both F1 and AUC metrics.

Conclusion

This paper introduces AEM, a novel approach to address attention concentration and overfitting in MIL frameworks. AEM incorporates a negative entropy regularization for attention values in the standard MIL framework. Our experimental results demonstrate the efficacy of AEM in mitigating attention concentration and overfitting. Compared to existing solutions, AEM offers notable advantages in its simplicity and versatility. It requires no additional modules or processing and involves only one hyperparameter, λ . Furthermore, AEM demonstrates enhanced performance when combined with various MIL frameworks and techniques. AEM’s simplicity and versatility position it as a potentially widely applicable enhancement to existing MIL methodologies in medical image analysis.

Limitation and future work. This paper primarily explores the effectiveness of AEM on the WSI classification task. In the future, we hope to further investigate extra tasks like survival prediction.

References

- Bejnordi, B. E.; Veta, M.; Van Diest, P. J.; Van Ginneken, B.; Karssemeijer, N.; Litjens, G.; Van Der Laak, J. A.; Hermesen, M.; Manson, Q. F.; Balkenhol, M.; et al. 2017. Diagnostic assessment of deep learning algorithms for detection of lymph node metastases in women with breast cancer. *Jama*, 318(22): 2199–2210.
- Bontempo, G.; Bolelli, F.; Porrello, A.; Calderara, S.; and Ficarra, E. 2023. A Graph-Based Multi-Scale Approach with Knowledge Distillation for WSI Classification. *TMI*.
- Chan, T. H.; Cendra, F. J.; Ma, L.; Yin, G.; and Yu, L. ??? Histopathology Whole Slide Image Analysis With Heterogeneous Graph Representation Learning. In *CVPR2023*.
- Dehaene, O.; Camara, A.; Moindrot, O.; de Lavergne, A.; and Courtiol, P. 2020. Self-supervision closes the gap between weak and strong supervision in histology. *arXiv preprint arXiv:2012.03583*.
- Dehghani, M.; Djolonga, J.; Mustafa, B.; Padlewski, P.; Heek, J.; Gilmer, J.; Steiner, A. P.; Caron, M.; Geirhos, R.; Alabdulmohsin, I.; et al. 2023. Scaling vision transformers to 22 billion parameters. In *ICML*, 7480–7512. PMLR.
- Ding, S.; Wang, J.; Li, J.; and Shi, J. 2023. Multi-scale prototypical transformer for whole slide image classification. In *MICCAI*, 602–611. Springer.
- Gadermayr, M.; Koller, L.; Tschuchnig, M.; Stangassinger, L. M.; Kreutzer, C.; Couillard-Despres, S.; Oostingh, G. J.; and Hittmair, A. 2023. Mixup-mil: Novel data augmentation for multiple instance learning and a study on thyroid cancer diagnosis. In *MICCAI*, 477–486. Springer.
- Grandvalet, Y.; and Bengio, Y. 2004. Semi-supervised learning by entropy minimization. *NeurIPS*, 17.
- Guan, Y.; Zhang, J.; Tian, K.; Yang, S.; Dong, P.; Xiang, J.; Yang, W.; Huang, J.; Zhang, Y.; and Han, X. 2022. Node-aligned graph convolutional network for whole-slide image representation and classification. In *CVPR*, 18813–18823.
- Guo, Z.; Zhao, W.; Wang, S.; and Yu, L. ??? HIGT: Hierarchical Interaction Graph-Transformer for Whole Slide Image Analysis. In *MICCAI2023*.
- He, K.; Zhang, X.; Ren, S.; and Sun, J. 2016. Deep residual learning for image recognition. In *CVPR*, 770–778.
- Hou, W.; Yu, L.; Lin, C.; Huang, H.; Yu, R.; Qin, J.; and Wang, L. 2022. H²-MIL: Exploring Hierarchical Representation with Heterogeneous Multiple Instance Learning for Whole Slide Image Analysis. In *AAAI*, volume 36, 933–941.
- Huang, Z.; Bianchi, F.; Yuksekgonul, M.; Montine, T. J.; and Zou, J. 2023. A visual-language foundation model for pathology image analysis using medical twitter. *Nature medicine*, 29(9): 2307–2316.
- Ikezogwo, W.; Seyfioglu, S.; Ghezloo, F.; Geva, D.; Sheikh Mohammed, F.; Anand, P. K.; Krishna, R.; and Shapiro, L. 2024. Quilt-1m: One million image-text pairs for histopathology. *NeurIPS*, 36.
- Ilse, M.; Tomczak, J.; and Welling, M. 2018. Attention-based deep multiple instance learning. In *ICML*, 2127–2136. PMLR.
- Kang, M.; Song, H.; Park, S.; Yoo, D.; and Pereira, S. 2023. Benchmarking Self-Supervised Learning on Diverse Pathology Datasets. In *CVPR*, 3344–3354.
- Keshvarikhajasteh, H.; Pluim, J. P.; and Veta, M. 2024. Multiple instance learning with random sampling for whole slide image classification. In *Medical Imaging 2024: Digital and Computational Pathology*, volume 12933, 372–376. SPIE.
- Keum, S.; Kim, S.; Lee, S.; and Lee, J. 2023. Slot-Mixup with Subsampling: A Simple Regularization for WSI Classification. *arXiv preprint arXiv:2311.17466*.
- Kingma, D. P.; and Welling, M. 2013. Auto-encoding variational bayes. *arXiv preprint arXiv:1312.6114*.
- Li, B.; Li, Y.; and Eliceiri, K. W. 2021. Dual-stream multiple instance learning network for whole slide image classification with self-supervised contrastive learning. In *CVPR*, 14318–14328.
- Li, B.; Liu, Z.; Shao, L.; Qiu, B.; Bu, H.; and Tian, J. 2024. Point Transformer with Federated Learning for Predicting Breast Cancer HER2 Status from Hematoxylin and Eosin-Stained Whole Slide Images. In *AAAI*, volume 38, 3000–3008.
- Li, H.; Zhang, Y.; Zhu, C.; Cai, J.; Zheng, S.; and Yang, L. 2023a. Long-MIL: Scaling Long Contextual Multiple Instance Learning for Histopathology Whole Slide Image Analysis. *arXiv preprint arXiv:2311.12885*.
- Li, H.; Zhu, C.; Zhang, Y.; Sun, Y.; Shui, Z.; Kuang, W.; Zheng, S.; and Yang, L. 2023b. Task-specific fine-tuning via variational information bottleneck for weakly-supervised pathology whole slide image classification. In *CVPR*, 7454–7463.
- Li, J.; Chen, W.; Huang, X.; Yang, S.; Hu, Z.; Duan, Q.; Metaxas, D. N.; Li, H.; and Zhang, S. 2021. Hybrid supervision learning for pathology whole slide image classification. In *MICCAI*, 309–318. Springer.
- Li, R.; Yao, J.; Zhu, X.; Li, Y.; and Huang, J. 2018. Graph CNN for survival analysis on whole slide pathological images. In *MICCAI*, 174–182. Springer.
- Lin, T.; Yu, Z.; Hu, H.; Xu, Y.; and Chen, C.-W. 2023. Interventional bag multi-instance learning on whole-slide pathological images. In *CVPR*, 19830–19839.
- Lin, W.; Zhuang, Z.; Yu, L.; and Wang, L. 2024. Boosting Multiple Instance Learning Models for Whole Slide Image Classification: A Model-Agnostic Framework Based on Counterfactual Inference. In *AAAI*, volume 38, 3477–3485.
- Lu, M. Y.; Chen, B.; Williamson, D. F.; Chen, R. J.; Liang, I.; Ding, T.; Jaume, G.; Odintsov, I.; Le, L. P.; Gerber, G.; et al. 2024. A visual-language foundation model for computational pathology. *Nature Medicine*, 30(3): 863–874.
- Lu, M. Y.; Williamson, D. F.; Chen, T. Y.; Chen, R. J.; Barbieri, M.; and Mahmood, F. 2021. Data-efficient and weakly

- supervised computational pathology on whole-slide images. *Nature biomedical engineering*, 5(6): 555–570.
- Ma, Y.; Luo, X.; Fu, K.; and Wang, M. 2024. Transformer-Based Video-Structure Multi-Instance Learning for Whole Slide Image Classification. In *AAAI*, volume 38, 14263–14271.
- McInnes, L.; Healy, J.; and Melville, J. 2018. Umap: Uniform manifold approximation and projection for dimension reduction. *arXiv preprint arXiv:1802.03426*.
- Miyato, T.; Maeda, S.-i.; Koyama, M.; and Ishii, S. 2018. Virtual adversarial training: a regularization method for supervised and semi-supervised learning. *IEEE TPAMI*, 41(8): 1979–1993.
- Myronenko, A.; Xu, Z.; Yang, D.; Roth, H. R.; and Xu, D. 2021. Accounting for dependencies in deep learning based multiple instance learning for whole slide imaging. In *MICCAI*, 329–338. Springer.
- Qu, L.; Wang, M.; Song, Z.; et al. 2022. Bi-directional weakly supervised knowledge distillation for whole slide image classification. *Neurips*, 35: 15368–15381.
- Radford, A.; Wu, J.; Child, R.; Luan, D.; Amodei, D.; Sutskever, I.; et al. 2019. Language models are unsupervised multitask learners. *OpenAI blog*, 1(8): 9.
- Rosenberg, A.; and Hirschberg, J. 2007. V-measure: A conditional entropy-based external cluster evaluation measure. In *EMNLP*, 410–420.
- Saito, K.; Kim, D.; Sclaroff, S.; Darrell, T.; and Saenko, K. 2019. Semi-supervised domain adaptation via minimax entropy. In *ICCV*, 8050–8058.
- Schulman, J.; Wolski, F.; Dhariwal, P.; Radford, A.; and Klimov, O. 2017. Proximal policy optimization algorithms. *arXiv preprint arXiv:1707.06347*.
- Shannon, C. E. 1948. A mathematical theory of communication. *The Bell system technical journal*, 27(3): 379–423.
- Shao, Z.; Bian, H.; Chen, Y.; Wang, Y.; Zhang, J.; Ji, X.; et al. 2021. Transmil: Transformer based correlated multiple instance learning for whole slide image classification. *Neurips*, 34: 2136–2147.
- Sharma, Y.; Shrivastava, A.; Ehsan, L.; Moskaluk, C. A.; Syed, S.; and Brown, D. 2021. Cluster-to-conquer: A framework for end-to-end multi-instance learning for whole slide image classification. In *MIDL*, 682–698. PMLR.
- Shi, X.; Xing, F.; Xie, Y.; Zhang, Z.; Cui, L.; and Yang, L. 2020. In *AAAI*, volume 34, 5742–5749.
- Song, A. H.; Jaume, G.; Williamson, D. F.; Lu, M. Y.; Vaidya, A.; Miller, T. R.; and Mahmood, F. 2023. Artificial intelligence for digital and computational pathology. *Nature Reviews Bioengineering*, 1(12): 930–949.
- Sun, Y.; Zhang, Y.; Si, Y.; Zhu, C.; Shui, Z.; Zhang, K.; Li, J.; Lyu, X.; Lin, T.; and Yang, L. 2024a. PathGen-1.6M: 1.6 Million Pathology Image-text Pairs Generation through Multi-agent Collaboration. *arXiv:2407.00203*.
- Sun, Y.; Zhu, C.; Zheng, S.; Zhang, K.; Sun, L.; Shui, Z.; Zhang, Y.; Li, H.; and Yang, L. 2024b. Pathasst: A generative foundation ai assistant towards artificial general intelligence of pathology. In *AAAI*, volume 38, 5034–5042.
- Tang, W.; Huang, S.; Zhang, X.; Zhou, F.; Zhang, Y.; and Liu, B. 2023. Multiple Instance Learning Framework with Masked Hard Instance Mining for Whole Slide Image Classification. *arXiv preprint arXiv:2307.15254*.
- Vaswani, A.; Shazeer, N.; Parmar, N.; Uszkoreit, J.; Jones, L.; Gomez, A. N.; Kaiser, Ł.; and Polosukhin, I. 2017. Attention is all you need. *NeurIPS*, 30.
- Wang, X.; Xiang, J.; Zhang, J.; Yang, S.; Yang, Z.; Wang, M.-H.; Zhang, J.; Yang, W.; Huang, J.; and Han, X. 2022. Scl-wc: Cross-slide contrastive learning for weakly-supervised whole-slide image classification. *NeurIPS*, 35: 18009–18021.
- Xiang, J.; and Zhang, J. 2022. Exploring low-rank property in multiple instance learning for whole slide image classification. In *ICLR*.
- Xiong, C.; Chen, H.; Sung, J.; and King, I. 2023. Diagnose Like a Pathologist: Transformer-Enabled Hierarchical Attention-Guided Multiple Instance Learning for Whole Slide Image Classification. *arXiv preprint arXiv:2301.08125*.
- Xiong, R.; Yang, Y.; He, D.; Zheng, K.; Zheng, S.; Xing, C.; Zhang, H.; Lan, Y.; Wang, L.; and Liu, T. 2020. On layer normalization in the transformer architecture. In *ICML*, 10524–10533. PMLR.
- Yang, J.; Chen, H.; Zhao, Y.; Yang, F.; Zhang, Y.; He, L.; and Yao, J. 2022. Remix: A general and efficient framework for multiple instance learning based whole slide image classification. In *MICCAI*, 35–45. Springer.
- Yao, J.; Zhu, X.; Jonnagaddala, J.; Hawkins, N.; and Huang, J. 2020. Whole slide images based cancer survival prediction using attention guided deep multiple instance learning networks. *MIA*, 65: 101789.
- Yufei, C.; Liu, Z.; Liu, X.; Liu, X.; Wang, C.; Kuo, T.-W.; Xue, C. J.; and Chan, A. B. 2022. Bayes-MIL: A New Probabilistic Perspective on Attention-based Multiple Instance Learning for Whole Slide Images. In *ICLR*.
- Zhai, S.; Likhomanenko, T.; Littwin, E.; Busbridge, D.; Ramapuram, J.; Zhang, Y.; Gu, J.; and Susskind, J. M. 2023. Stabilizing transformer training by preventing attention entropy collapse. In *ICML*, 40770–40803. PMLR.
- Zhang, H.; Meng, Y.; Zhao, Y.; Qiao, Y.; Yang, X.; Coupland, S. E.; and Zheng, Y. 2022a. DTFD-MIL: Double-tier feature distillation multiple instance learning for histopathology whole slide image classification. In *CVPR*, 18802–18812.
- Zhang, J.; Zhang, X.; Ma, K.; Gupta, R.; Saltz, J.; Vakalopoulou, M.; and Samaras, D. 2022b. Gigapixel whole-slide images classification using locally supervised learning. In *MICCAI*, 192–201. Springer.
- Zhang, Y.; Li, H.; Sun, Y.; Zheng, S.; Zhu, C.; and Yang, L. 2024. Attention-Challenging Multiple Instance Learning for Whole Slide Image Classification. *ECCV*.
- Zhang, Y.; Sun, Y.; Li, H.; Zheng, S.; Zhu, C.; and Yang, L. 2022c. Benchmarking the robustness of deep neural networks to common corruptions in digital pathology. In *MICCAI*, 242–252. Springer.

Zhao, W.; Wang, S.; Yeung, M.; Niu, T.; and Yu, L. 2023. MulGT: multi-task graph-transformer with task-aware knowledge injection and domain knowledge-driven pooling for whole slide image analysis. In *AAAI*, volume 37, 3606–3614.

Zhao, Y.; Yang, F.; Fang, Y.; Liu, H.; Zhou, N.; Zhang, J.; Sun, J.; Yang, S.; Menze, B.; Fan, X.; et al. 2020. Predicting lymph node metastasis using histopathological images based on multiple instance learning with deep graph convolution. In *CVPR*, 4837–4846.

Zheng, Y.; Li, J.; Shi, J.; Xie, F.; and Jiang, Z. ??? Kernel attention transformer (KAT) for histopathology whole slide image classification. In *MICCAI2022*.

Zhou, B.; Khosla, A.; Lapedriza, A.; Oliva, A.; and Torralba, A. 2016. Learning deep features for discriminative localization. In *CVPR*, 2921–2929.

Experimental setup

Datasets and Evaluation Metrics.

The performance of AEM is evaluated on two public WSI datasets, i.e., CAMELYON16 (Bejnordi et al. 2017) and CAMELYON17 (Bejnordi et al. 2017), and one private dataset, LBC. CAMELYON16 dataset consists of 400 WSIs in total, including 270 for training and 130 for testing. Following (Zhang et al. 2022a; Li, Li, and Eliceiri 2021; Zhang et al. 2024), we further randomly split the training and validation sets from the official training set with a ratio of 9:1. CAMELYON17 dataset contains 1,000 WSIs collected from five hospitals, categorized into different slide labels such as Normal, isolated tumor cells, Micro-metastases, and Macro-metastases. Due to the absence of labels for the test set, the training set (500 WSIs) is reallocated to validate the OOD performance. Specifically, 200 WSIs from the fourth and fifth hospitals are designated as the test set, while the remaining 300 WSIs are randomly split for training and validation in a 9:1 ratio. The liquid-based cytology (LBC) dataset collected 1,989 WSIs and included 4 classes, i.e., Negative, ASC-US, LSIL, and ASC-H/HSIL. We randomly split the whole dataset into training, validation, and test sets with the ratio of 6:2:2. Following (Li et al. 2023b; Zhang et al. 2024), macro-AUC and macro-F1 scores are reported. Each main experiment is conducted five times with random parameter initializations, and the average classification performance and standard deviation are reported. Besides, following (Lu et al. 2021; Zhang et al. 2022a, 2024), the test performance is reported in epochs with the best validation performance.

Implementation Details of AEM.

(1) *Pre-processing*. We follow the pre-processing of CLAM (Lu et al. 2021), which involves threshold segmentation and filtering to locate tissue regions in each WSI. From these regions, we extract non-overlapping patches of size 256×256 at a magnification of $\times 20$. (2) *Model Architecture*. Learnable components of the model include one fully-connected layer to reduce features to 128 dimensions, a gated attention network, and a fully-connected layer for making predictions.

(3) *Optimization*. The model is trained for 50 epochs using a cosine learning rate decay starting at 0.0001. We employ an Adam optimizer with a weight decay of 0.0001, and the batch size is set to 1. (4) *Hyperparameters*. The default λ is determined based on the validation performance. In this paper, the default λ is set as 0.005, 0.1, and 0.1 for CAMELYON16, CAMELYON17, and LBC, respectively.

Implementation Details of Subsampling and Integration with AEM

Subsampling (Keum et al. 2023; Keshvarikhajasteh, Pluim, and Veta 2024) is a simple yet effective augmentation technique in MIL for WSI classification. This technique aims to improve model generalization and computational efficiency by working with a subset of instances from each bag.

Subsampling Technique The subsampling process randomly selects a portion of instances (i.e., $r \times 100\%$) from each bag during training. Formally, for a bag $X = \{x_1, x_2, \dots, x_N\}$ with N instances, we create a subsampled bag $X' = \{x'_1, x'_2, \dots, x'_M\}$, where $M = \lfloor rN \rfloor$ and each x'_i is randomly selected from X without replacement.

In our implementation, we perform subsampling dynamically for each epoch, which introduces variability in the training process and helps prevent overfitting. We explore a range of subsampling ratios:

$$r \in \{0.2, 0.4, 0.6, 0.8\}. \quad (6)$$

The optimal value of r is selected based on the model’s performance on the validation set.

Integration with AEM While subsampling operates on the instance selection level, AEM works as a regularization term. As such, integrating AEM with subsampling is straightforward and equivalent to combining AEM with the base ABMIL.

The AEM loss is applied to the attention weights of the subsampled instances:

$$\mathcal{L}_{aem} = \sum_{i=1}^M a_i \log a_i, \quad (7)$$

where a_i is the attention weight for the i -th instance in the subsampled bag.

The overall loss function becomes:

$$\mathcal{L} = \mathcal{L}_{mil} + \lambda_{aem} \mathcal{L}_{aem}, \quad (8)$$

where \mathcal{L}_{mil} is the standard MIL loss (e.g., cross-entropy), and λ_{aem} is a hyperparameter controlling the contribution of the AEM loss.

Implementation Details of DTFD-MIL and Integration with AEM

The DTFD-MIL method introduces a double-tier framework for WSI classification, designed to enlarge the number of bags by introducing the concept of pseudo-bags.

DTFD-MIL Framework Each slide (bag) X is first split into M pseudo-bags $\{X^1, X^2, \dots, X^M\}$. The number of pseudo-bags M is typically determined based on the size of the WSI and computational resources available, balancing between fine-grained analysis and efficiency.

Tier-1 MIL: An Attention-Based MIL (ABMIL) model is applied to each pseudo-bag:

$$F^j = \sum_{k=1}^{K_j} a_k^j h_k^j, \quad (9)$$

where F^j is the feature representation of the j -th pseudo-bag, a_k^j is the attention score, and h_k^j is the feature of the k -th instance in this pseudo-bag. This tier captures local patterns within each pseudo-bag.

Tier-2 MIL: The Class Activation Mapping (CAM) (Zhou et al. 2016) technique is applied to distill critical instances from each pseudo-bag. CAM generates heatmaps highlighting discriminative regions, allowing us to focus on the most informative areas. Another ABMIL model is then applied to these distilled features:

$$F = \sum_{j=1}^M a_j F^j, \quad (10)$$

where F is the final representation of the slide. This tier captures global patterns across pseudo-bags.

Both tiers are supervised by the slide-level label Y_i :

$$\mathcal{L} = \mathcal{L}_1 + \mathcal{L}_2, \quad (11)$$

where \mathcal{L}_1 and \mathcal{L}_2 are the losses for Tier-1 and Tier-2, respectively. We use binary cross-entropy loss for both tiers:

$$\mathcal{L}_i = -Y_i \log(\hat{Y}_i) - (1 - Y_i) \log(1 - \hat{Y}_i), \quad (12)$$

where \hat{Y}_i is the predicted probability for the i -th slide.

Integration with AEM We combine Attention Entropy Maximization (AEM) with DTFD-MIL by applying it to Tier-1 MIL. This choice is motivated by the fact that Tier-1 operates on a larger number of instances, where attention distribution is more critical. The AEM in DTFD-MIL is defined as:

$$\mathcal{L}_{aem} = \frac{1}{M} \sum_{j=1}^M \sum_{k=1}^{K_j} a_k^j \log a_k^j. \quad (13)$$

AEM encourages a more uniform distribution of attention values, preventing over-concentration on a few instances and potentially improving the model's ability to capture diverse patterns.

The overall loss formulation becomes:

$$\mathcal{L} = \mathcal{L}_1 + \mathcal{L}_2 + \lambda_{aem} \mathcal{L}_{aem}, \quad (14)$$

where λ_{aem} is a hyperparameter controlling the contribution of the AEM loss. In our experiments, we typically set λ_{aem} to its default setting in the ABMIL. For the hyperparameter of DTFD-MIL, we set the number of pseudo-bags $M = 4$ and use the MaxMin selection.

Implementation Details of AC MIL and Integration with AEM

AC MIL consists of two main components designed to address attention value concentration and mitigate overfitting in WSI classification:

Multiple Branch Attention (MBA) MBA captures diverse discriminative instances using M attention branches. Each branch i generates a bag embedding \mathbf{z}_i :

$$\mathbf{z}_i = \sum_{n=1}^N a_{in} \mathbf{h}_n, \quad (15)$$

where a_{in} is the attention value for instance n in branch i , and \mathbf{h}_n is the instance embedding.

To ensure each branch captures specific discriminative features, we introduce semantic loss \mathcal{L}_p and diversity loss \mathcal{L}_d :

$$\mathcal{L}_p = -\frac{1}{M} \sum_{i=1}^M \mathbf{Y} \log \hat{\mathbf{Y}}_i + (1 - \mathbf{Y}) \log(1 - \hat{\mathbf{Y}}_i), \quad (16)$$

$$\mathcal{L}_d = \frac{2}{M(M-1)} \sum_{i=1}^M \sum_{j=i+1}^M \cos(\mathbf{a}_i, \mathbf{a}_j), \quad (17)$$

where \mathbf{Y} is the true label, $\hat{\mathbf{Y}}_i$ is the prediction from branch i , and \mathbf{a}_i is the attention vector for branch i .

The features captured by attention branches are integrated using mean-pooling for the final slide prediction:

$$\mathbf{z} = \frac{1}{M} \sum_{i=1}^M \mathbf{z}_i. \quad (18)$$

The bag classification loss \mathcal{L}_b is then computed as:

$$\mathcal{L}_b = -\mathbf{Y} \log \hat{\mathbf{Y}} + (1 - \mathbf{Y}) \log(1 - \hat{\mathbf{Y}}), \quad (19)$$

where $\hat{\mathbf{Y}}$ is the final prediction based on \mathbf{z} .

Stochastic Top-K Instance Masking (STKIM) STKIM addresses over-reliance on a small subset of salient instances by randomly masking out instances with top-K attention values. The modified attention values are:

$$a_n = \begin{cases} 0, & \text{with probability } p \text{ if } a_n \text{ is in top-K} \\ a_n, & \text{otherwise} \end{cases} \quad (20)$$

After masking, the remaining attention values are normalized to sum to 1, effectively redistributing the attention to non-masked instances.

Integration with AEM We integrate AEM into AC MIL by applying it to each attention branch. The AEM loss is defined as:

$$\mathcal{L}_{aem} = \frac{1}{M} \sum_{i=1}^M \sum_{n=1}^N a_{in} \log a_{in}. \quad (21)$$

AEM encourages a more uniform distribution of attention values, complementing STKIM in preventing over-concentration in a few instances.

Final Optimization Objective The final loss function combines all components:

$$\mathcal{L} = \mathcal{L}_b + \mathcal{L}_p + \mathcal{L}_d + \lambda_{aem} \mathcal{L}_{aem}, \quad (22)$$

where λ_{aem} are hyperparameters controlling the contribution of \mathcal{L}_{aem} .

In our experiments, according to the original paper, we use $M = 5$ attention branches and set $K = 10$ for STKIM. The masking probability p is set to 0.6. These hyperparameters can be adjusted based on the specific dataset and task requirements.

Implementation Details of DSMIL and Integration with AEM

DSMIL Framework DSMIL consists of two parallel streams that jointly learn instance-level and bag-level representations.

Formally, given a bag of instances $B = \{x_1, x_2, \dots, x_N\}$, DSMIL processes them as follows:

$$h_i = f(x_i), \quad i = 1, \dots, N, \quad (23)$$

where $f(\cdot)$ is a feature extractor that maps each instance to an embedding space.

The first stream employs max-pooling to identify the most discriminative instance:

$$c_m(B) = \max_i W_0 h_i, \quad (24)$$

where W_0 is a learnable weight matrix.

The second stream computes attention weights based on the similarity to the most discriminative instance:

$$U(h_i, h_m) = \frac{\exp(\langle q_i, q_m \rangle)}{\sum_{k=1}^N \exp(\langle q_k, q_m \rangle)}, \quad (25)$$

where $q_i = W_q h_i$ and h_m is the embedding of the instance with the highest score from the first stream.

The bag-level representation is then computed as:

$$b = \sum_{i=1}^N U(h_i, h_m) v_i, \quad (26)$$

where $v_i = W_v h_i$ are instance information vectors.

Integration of DSMIL and AEM To integrate DSMIL with AEM, we apply the AEM loss to the attention weights $U(h_i, h_m)$:

$$\mathcal{L}_{aem} = \sum_{i=1}^N U(h_i, h_m) \log U(h_i, h_m) \quad (27)$$

The final loss function becomes:

$$\mathcal{L} = \mathcal{L}_{dsmil} + \lambda_{aem} \mathcal{L}_{aem}, \quad (28)$$

where \mathcal{L}_{dsmil} is the original DSMIL loss and λ_{aem} is a hyperparameter controlling the AEM contribution.

Implementation Details of Multi-Head Attention and Integration with AEM

Multi-Head Attention (MHA) (Vaswani et al. 2017) is a powerful mechanism that has shown great success in various deep learning tasks, including MIL for WSI classification. This technique allows the model to jointly attend to information from different representation subspaces at different positions.

Multi-Head Attention Technique In the context of MIL, given a bag of instance embeddings $X = \{x_1, x_2, \dots, x_N\}$ where $x_i \in \mathbb{R}^d$, MHA performs the following operations:

$$\text{MHA}(X) = \text{Concat}(\text{head}_1, \dots, \text{head}_h) W^O, \quad (29)$$

where each head is computed as:

$$\text{head}_i = \text{Attention}(X W_i^Q, X W_i^K, X W_i^V). \quad (30)$$

The attention function is defined as:

$$\text{Attention}(Q, K, V) = \text{softmax}\left(\frac{QK^T}{\sqrt{d_k}}\right)V. \quad (31)$$

Here, $W_i^Q, W_i^K, W_i^V \in \mathbb{R}^{d \times d_k}$ and $W^O \in \mathbb{R}^{hd_k \times d}$ are learnable parameters, and h is the number of attention heads. In our implementation, we choose the commonly used head number of 8.

Integration with AEM Integrating AEM with MHA is straightforward, as we can apply the AEM loss to the attention weights produced by each head. The AEM loss for MHA becomes:

$$\mathcal{L}_{aem} = \frac{1}{h} \sum_{j=1}^h \sum_{i=1}^N a_{i,j} \log a_{i,j}, \quad (32)$$

where $a_{i,j}$ is the attention weight for the i -th instance in the j -th attention head.

The overall loss function is then:

$$\mathcal{L} = \mathcal{L}_{mil} + \lambda_{aem} \mathcal{L}_{aem}, \quad (33)$$

where \mathcal{L}_{mil} is the standard MIL loss, and λ_{aem} is a hyperparameter controlling the contribution of the AEM loss.

Additional experiments

AEM effectively mitigates the attention concentration.

Figure 9 demonstrates how AEM effectively mitigates the attention concentration problem observed in ABMIL for the LBC test set. The ABMIL curve (blue) rises sharply, indicating that it focuses most of its attention on a small subset of patches. In contrast, the AEM curve (brown) shows a much more gradual increase, suggesting a more balanced distribution of attention across a larger number of patches.

Table 3: The performance of different MIL approaches across three datasets and two evaluation metrics on ImageNet pretrained ResNet18 and VLP pretrained ViT-B. The most superior performance is highlighted in **bold**.

ImageNet pretrained ResNet18 ((He et al. 2016))						
Method	CAMELYON-16		CAMELYON-17		LBC	
	F1-score	AUC	F1-score	AUC	F1-score	AUC
ABMIL (Ilse, Tomczak, and Welling 2018)	0.759 \pm 0.012	0.797 \pm 0.026	0.481 \pm 0.046	0.798\pm0.008	0.469 \pm 0.029	0.741 \pm 0.020
AEM(ours)	0.769\pm0.018	0.804\pm0.027	0.482\pm0.035	0.797 \pm 0.009	0.532\pm0.019	0.818\pm0.013
VLP pretrained ViT-B (PathGen-CLIP (Sun et al. 2024a))						
Method	CAMELYON-16		CAMELYON-17		LBC	
	F1-score	AUC	F1-score	AUC	F1-score	AUC
ABMIL (Ilse, Tomczak, and Welling 2018)	0.944 \pm 0.012	0.970\pm0.008	0.557 \pm 0.020	0.862 \pm 0.015	0.569 \pm 0.020	0.821 \pm 0.016
AEM(ours)	0.949\pm0.011	0.964 \pm 0.015	0.673\pm0.023	0.890\pm0.007	0.602\pm0.027	0.844\pm0.019

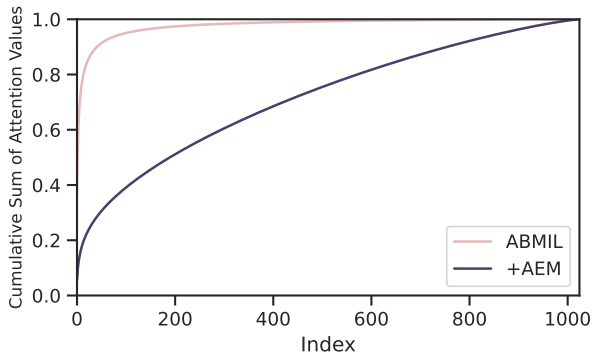


Figure 9: The mean cumulative sum of top-1000 attention values for the LBC test set. Index 1 gets the highest attention score among patches.

Heatmap Visualization.

The heatmap can identify important instances that provide insight into the prediction. In clinical practice, the heatmap is always used to ensure the reliability of the method by comparing it with expert knowledge and serve as an indicator for the automatic selection of regions of interest (Song et al. 2023). Figure 10 presents heatmap visualizations illustrating three examples of our AEM compared to the baseline method, ABMIL (Ilse, Tomczak, and Welling 2018).

In the first WSI, a large tumor region is present. Contrasting with ABMIL, AEM disperses attention across a broader range of tumor instances. Moving to the second and third WSIs, which contain smaller tumor regions, ABMIL concentrates solely on a part of tumor instances, whereas AEM effectively identifies the entire tumor region.

Performance on ImageNet pretrained ResNet18 and VLP pretrained ViT-B

Table 3 presents a comparative analysis of MIL approaches across three datasets (CAMELYON-16, CAMELYON-17, and LBC) using two different backbone architectures (ImageNet pretrained ResNet18 and VLP pretrained ViT-B) and two evaluation metrics (F1-score and AUC).

A key finding is that AEM, our proposed method, consistently demonstrates superior performance, particularly in more challenging tasks. This is evidenced by the improvements observed across various scenarios, especially in the more difficult CAMELYON-17 and LBC datasets.

With ImageNet pretrained ResNet18, AEM achieves higher F1-scores for all three datasets, with notable improvements in the LBC dataset (0.532 vs 0.469). Using VLP pretrained ViT-B, AEM’s effectiveness becomes even more pronounced. For CAMELYON-17, AEM significantly improves the F1-score from 0.557 to 0.673, a substantial 20.8% relative increase. This remarkable enhancement in a challenging dataset highlights AEM’s capacity to extract more discriminative features and make more accurate predictions in complex scenarios.

These consistent improvements across different architectures and datasets, particularly in more difficult tasks, underscore AEM’s robustness and its potential to advance the state-of-the-art in medical image analysis tasks of varying complexity.

AEM learns more discriminative bag features.

We employ UMAP visualization to visualize the discriminative ability of bag features learned by ABMIL and AEM. In Figure 11a, we see a less distinct separation between categories. The red-circled cluster in the upper left shows a mix of LSIL, ASC-H/HSIL, and some ASC-US points, but they’re not clearly separated from the main cluster of Negative points. In contrast, plot (b) AEM (V-measure=0.302) demonstrates a more pronounced separation of categories. The red-circled cluster on the left side is more compact and better isolated from the Negative samples, indicating improved discrimination of abnormal bags. The higher V-measure for AEM (0.302 vs 0.276) quantitatively confirms the improved clustering performance.

More analysis of integrating AEM into DTFD-MIL, ACML, and Subsampling.

Compared to Figure 7 in the main paper, we further supplement the results of the F1-scores and standard deviation

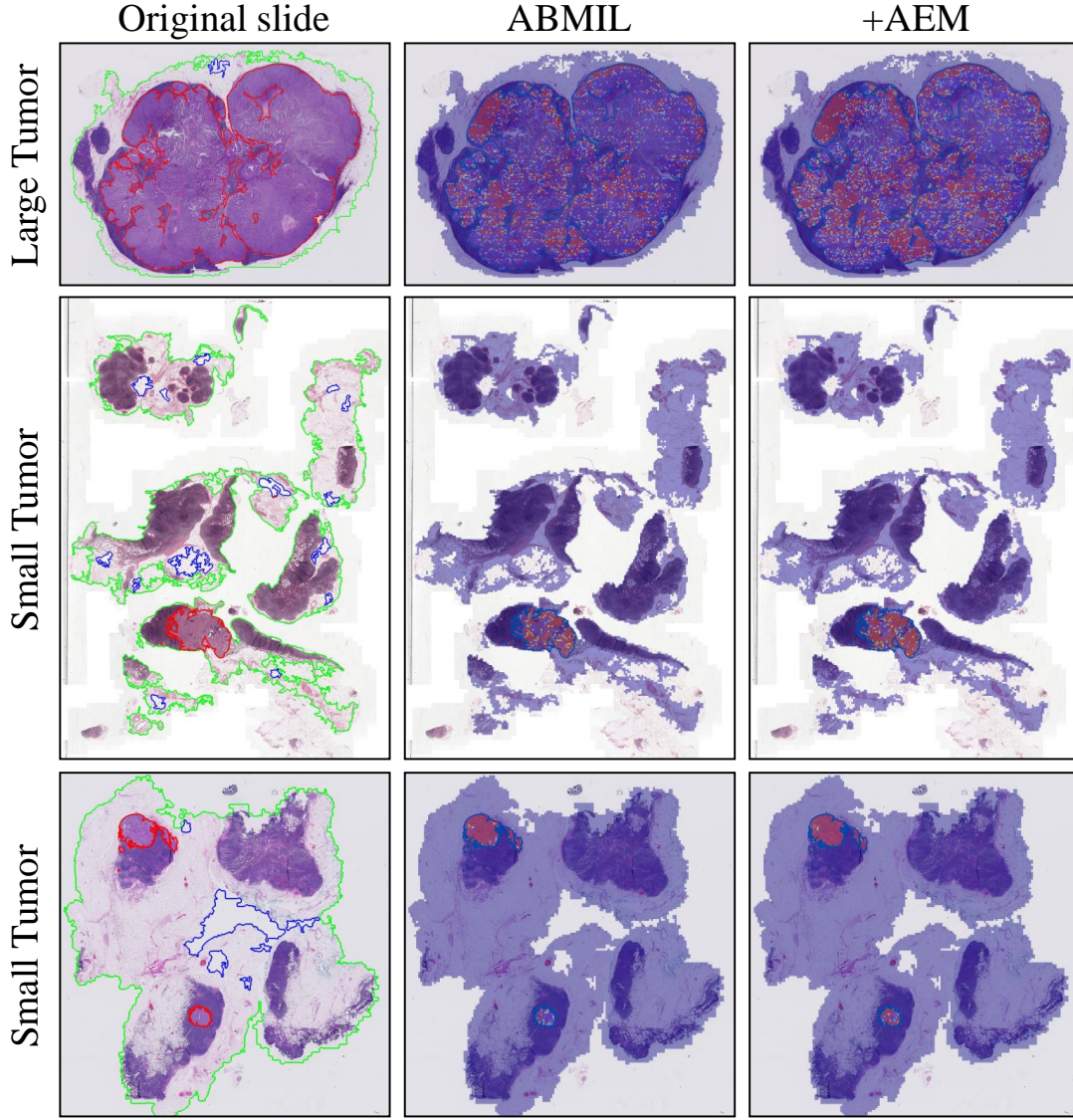


Figure 10: Heatmap visualization of WSIs produced by ABMIL and AEM (Zoom-in for best view). We selected three WSIs from the CAMELYON16 dataset: one slide with large tumor regions and two slides with small tumor regions. AEM assigns attention values to a broader range of tumor instances compared to ABMIL, leading to better alignment with expert annotations.

information in Table 4. We use the unpaired t-test to analyze the performance comparison between methods with and without AEM.

For the Subsampling method, AEM consistently improves performance across all datasets and backbones. On CAMELYON-16, it significantly enhances the F1-score (from 0.930 to 0.950, $p < 0.05$) with SSL pretrained ViT-S, and both AUC and F1-score with VLP pretrained ViT-L. For CAMELYON-17, substantial improvements are observed in both AUC and F1-score across both backbones (e.g., AUC: 0.853 to 0.888, F1: 0.512 to 0.646 with SSL pretrained ViT-S, both $p < 0.05$). On LBC, AEM yields significant enhancements, particularly with SSL pretrained ViT-S (AUC: 0.823 to 0.876, F1: 0.605 to 0.658, both $p < 0.05$).

For the DTFD-MIL method, AEM demonstrates con-

sistent improvements across datasets and backbones. On CAMELYON-16, it slightly improves AUC with SSL pretrained ViT-S (0.976 to 0.982) and both metrics with VLP pretrained ViT-L. For CAMELYON-17, AEM significantly boosts both AUC and F1-score across both backbones (e.g., AUC: 0.870 to 0.891, F1: 0.547 to 0.578 with SSL pretrained ViT-S, both $p < 0.05$). On LBC, substantial improvements are observed, especially with SSL pretrained ViT-S (AUC: 0.842 to 0.872, F1: 0.612 to 0.656, both $p < 0.01$).

For the ACMIL method, AEM’s impact varies but shows general improvement. On CAMELYON-16, changes are minimal with SSL pretrained ViT-S, but show improvement with VLP pretrained ViT-L. For CAMELYON-17, AEM significantly improves both metrics across both backbones (e.g., AUC: 0.873 to 0.887, F1: 0.550 to 0.603 with SSL pre-

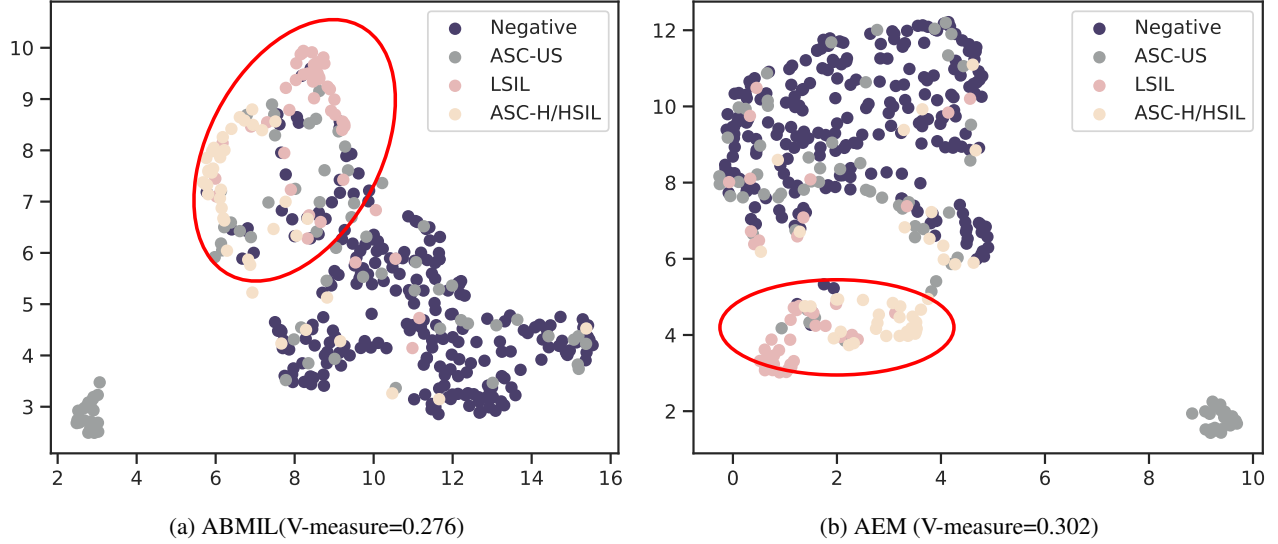


Figure 11: UMAP visualization (McInnes, Healy, and Melville 2018) of bag features for LBC test set. AEM effectively learns more discriminative features than ABMIL by improving the separation of ‘LSIL’ and ‘ASC-H/HSIL’ features from the ‘Negative’ class (highlighted by a red ellipse). Improving feature separation is also corroborated by the V-measure score (Rosenberg and Hirschberg 2007), a clustering metric that considers both the homogeneity and completeness of the clusters.

Table 4: Performance comparison of three MIL methods (subsampling, DTFD-MIL, and AC MIL) with and without AEM integration on three datasets and two backbones. Bold values indicate statistically significant improvements (P-value of Unpaired t-test less than 0.05) between the base method and its AEM-integrated version.

SSL pretrained ViT-S (Lunit (Kang et al. 2023))						
Method	CAMELYON-16		CAMELYON-17		LBC	
	AUC	F1-score	AUC	F1-score	AUC	F1-score
subsampling (Keum et al. 2023)	0.980 \pm 0.010	0.930 \pm 0.012	0.853 \pm 0.014	0.512 \pm 0.041	0.823 \pm 0.014	0.605 \pm 0.038
subsampling+AEM	0.980 \pm 0.010	0.950\pm0.008	0.888\pm0.010	0.646\pm0.055	0.876\pm0.012	0.658\pm0.045
DTFD-MIL (Zhang et al. 2022a)	0.976 \pm 0.007	0.957 \pm 0.007	0.870 \pm 0.021	0.547 \pm 0.037	0.842 \pm 0.011	0.612 \pm 0.033
DTFD-MIL+AEM	0.982\pm0.013	0.948 \pm 0.011	0.891\pm0.012	0.578\pm0.029	0.872\pm0.010	0.656\pm0.024
AC MIL (Zhang et al. 2024)	0.978 \pm 0.010	0.940 \pm 0.011	0.873 \pm 0.019	0.550 \pm 0.054	0.897 \pm 0.011	0.655 \pm 0.033
AC MIL+AEM	0.978 \pm 0.009	0.939 \pm 0.012	0.887\pm0.004	0.603\pm0.014	0.898 \pm 0.012	0.657 \pm 0.024
VLP pretrained ViT-L (PathGen-CLIP (Sun et al. 2024a))						
Method	CAMELYON-16		CAMELYON-17		LBC	
	F1-score	AUC	F1-score	AUC	F1-score	AUC
subsampling (Keum et al. 2023)	0.982 \pm 0.013	0.948 \pm 0.025	0.904 \pm 0.010	0.644 \pm 0.035	0.881 \pm 0.009	0.666 \pm 0.014
subsampling+AEM	0.989 \pm 0.006	0.956 \pm 0.019	0.916\pm0.006	0.689\pm0.013	0.885 \pm 0.008	0.684 \pm 0.028
DTFD-MIL (Zhang et al. 2022a)	0.978 \pm 0.010	0.955 \pm 0.009	0.907 \pm 0.009	0.657 \pm 0.009	0.874 \pm 0.012	0.650 \pm 0.036
DTFD-MIL+AEM	0.987 \pm 0.005	0.965 \pm 0.011	0.924\pm0.008	0.678\pm0.018	0.893\pm0.007	0.688\pm0.025
AC MIL (Zhang et al. 2024)	0.979 \pm 0.010	0.918 \pm 0.012	0.926 \pm 0.007	0.628 \pm 0.035	0.891 \pm 0.010	0.683 \pm 0.028
AC MIL+AEM	0.982 \pm 0.010	0.926 \pm 0.019	0.936\pm0.008	0.672\pm0.064	0.891 \pm 0.011	0.677 \pm 0.028

trained ViT-S, $p < 0.05$). On LBC, improvements are modest but consistent, with slight enhancements in both AUC and F1-score.

Overall, AEM can achieve comparable performance or significantly improve the performance upon three methods. Especially for the more difficult datasets, CAMELYON-

17 and LBC, AEM demonstrates consistent and substantial improvements across all methods and backbones. This suggests that AEM is particularly effective in enhancing model performance on challenging datasets where traditional MIL methods may struggle. The results indicate that AEM is a robust technique that can be successfully inte-

grated with various MIL approaches and backbone architectures to boost their performance, particularly in complex classification tasks.